Eur. Phys. J. D **33**, 161–171 (2005)
DOI: 10.1140/epjd/e2005-00058-0

THE EUROPEAN PHYSICAL JOURNAL D

Accurate spectroscopy of Sr atoms

I. Courtillot, A. Quessada-Vial, A. Brusch, D. Kolker, G.D. Rovera, and P. Lemonde[a]

BNM-SYRTE, Observatoire de Paris, 61 avenue de l'observatoire, 75014 Paris, France

Received 16 October 2004 / Received in final form 31 January 2005
Published online 3 May 2005 –

Abstract. We report the frequency measurement with an accuracy in the 100 kHz range of several optical transitions of atomic Sr: $^1S_0-^3P_1$ at 689 nm, $^3P_1-^3S_1$ at 688 nm and $^3P_0-^3S_1$ at 679 nm. Measurements are performed with a frequency chain based on a femtosecond laser referenced to primary frequency standards. They allowed the indirect determination with a 70 kHz uncertainty of the frequency of the doubly forbidden $5s^2\ ^1S_0 - 5s5p\ ^3P_0$ transition of ^{87}Sr at 698 nm and in a second step its direct observation. Frequency measurements are performed for ^{88}Sr and ^{87}Sr, allowing the determination of $^3P_0$, $^3P_1$ and $^3S_1$ isotope shifts, as well as the $^3S_1$ hyperfine constants.

PACS. 06.30.Ft Time and frequency – 32.30.Jc Visible and ultraviolet spectra – 39.30.+w Spectroscopic techniques – 32.80.-t Photon interactions with atoms

1 Introduction

Precise measurements of the energy of atomic levels is of extreme importance for modern physics. To quote a few examples, for simple atoms (H, He...) they lead to accurate tests of quantum electrodynamics and give access to fundamental constants such as the Rydberg constant [1–5]. For more complex systems they give rise to new generations of atomic clocks with the perspective of an improved definition of the SI second (see e.g. [6]), they allow stringent laboratory tests of local position invariance [7–11] and combined with mass ratio measurements they lead to accurate determinations of the fine structure constant α [12–15].

Many of the atomic transitions of interest lie in the optical domain of the electromagnetic spectrum. In the heroic times of optical frequency metrology, measurements were based on phase coherent harmonic frequency chains which required a specific complex apparatus for each transition under consideration [16–21]. Very few atomic or molecular resonances have been measured directly with this technique [22]. A few more transitions have been indirectly measured with decent accuracy thanks to their coincidental vicinity to one of these few references. The vast majority of atomic transitions however are only known to within a few hundred MHz, limited by the mechanical quality of spectrometers. The situation has dramatically changed over the last few years with the advent of optical frequency combs [22,23]. Very compact and simple apparatus are now available which in principle allow the phase coherent comparison of any frequencies ranging from the GHz to the PHz domain.

[a] e-mail: pierre.lemonde@obspm.fr

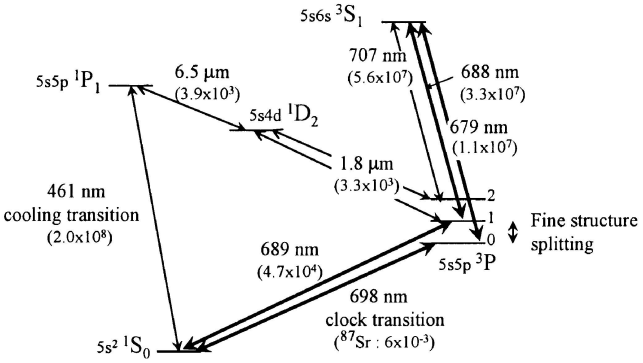

Fig. 1. Energy diagram of Sr with wavelength and decay rate (s^{-1}) of the transitions involved in the experiment. Two isotopes have been studied, ^{88}Sr and ^{87}Sr of natural abundance 82% and 7% respectively. ^{87}Sr possesses a hyperfine structure ($I = 9/2$) which is not shown here for clarity. The 698 nm transition is weakly allowed for ^{87}Sr by hyperfine coupling.

We describe here the extensive use of this technique for the spectroscopy of Sr atoms. We report the frequency measurement with an accuracy in the hundred kHz range of the $^1S_0-^3P_1$, $^3P_1-^3S_1$ and $^3P_0-^3S_1$ transitions at 689, 688 and 679 nm respectively (see Fig. 1). The measurements are performed with both 88 and 87 isotopes. For the latter, hyperfine components have been measured giving access to the hyperfine parameters of the $^3S_1$ state and to the isotope shifts of $^3P_0$, $^3P_1$ and $^3S_1$. The interest of these measurements is illustrated by the first observation of the $^1S_0 - ^3P_0$ transition of ^{87}Sr which we have reported in [24]. This was made possible by the indirect determination of the $^3P_0$ state energy given by the measurements

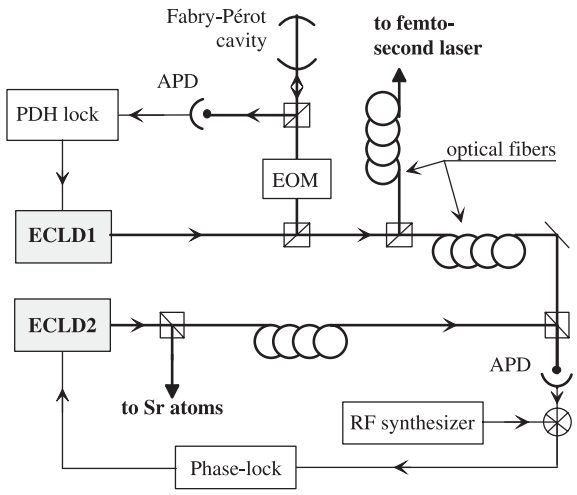

Fig. 2. Experimental set-up used for frequency measurements. A first extended cavity laser diode (ECLD1) is locked to a high finesse Fabry-Pérot cavity. 100 μW of its output power are sent to a frequency chain based on a femtosecond laser for absolute frequency measurement. A second laser (ECLD2), offset-phase locked to ECDL1, is used to probe the strontium atoms. Noise and frequency offsets introduced by optical fibers are negligible in this experiment. EOM: electro-optical modulator.

detailed here. The direct frequency measurement with a 15 kHz accuracy of this transition in turn nicely confirms the indirect determination. It also opens the way to a new generation of optical frequency standards with atoms confined in a dipole trap [25].

2 Experimental set-up

All frequency measurements were performed with the experimental set-up sketched in Figure 2. An extended cavity laser diode (ECLD1) is locked to a high finesse cavity using the Pound-Drever-Hall method [26] with performances reported in reference [27]. This laser has a linewidth of 35 Hz. Its absolute frequency is continuously measured vs. BNM-SYRTE primary frequency standards with a scheme based on a self referenced femtosecond Ti:Sa laser [22,23]. The fractional resolution of this measurement is typically 3×10^{-13} for a one second averaging time (corresponding to 100 Hz in the region of the spectrum involved here). ECLD1 is used as a frequency reference for a second laser, ECLD2, that probes the strontium atoms. ECLD2 is offset-phase locked to ECLD1: the beat-note between both lasers is detected by an avalanche photodiode (APD) and mixed with the output of a radio-frequency synthesizer to generate the offset phase lock error signal. The bandwidth of the servo control is 2 MHz. By actuating the RF synthesizer, the light of ECLD2 which is sent to the atoms can be continuously tuned to any frequency between two modes of the cavity of free spectral range 1.5 GHz. This point was of importance for the first detection of the transitions since their frequencies were not accurately known. To measure all the atomic resonances, two sets of lasers are used. The first set can be tuned from 675 to 685 nm, the second one from 685 to 698 nm.

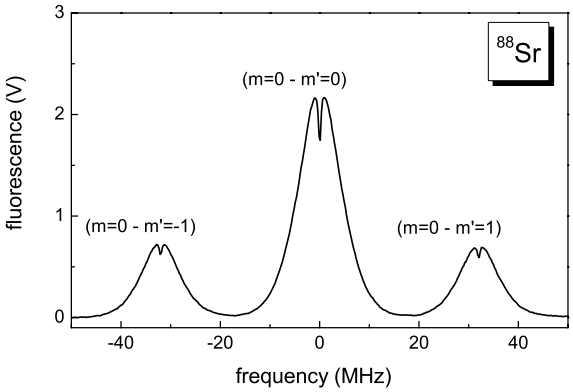

Fig. 3. $^1S_0 - {}^3P_1$ resonance of ^{88}Sr. The Lamb dip at the center of the Doppler profile is broadened by saturation to 550 kHz. All three Zeeman components are visible on this scan.

Except for the $^1S_0 - {}^3P_1$ transition, the frequency measurements are made by probing a sample of cold atoms collected in a magneto-optical trap (MOT). An atomic beam is decelerated in a Zeeman slower and captured at the crossing-point of three retro-reflected beams tuned to the red of the $^1S_0 - {}^1P_1$ transition at 461 nm. The set-up is detailed in reference [28]. For these experiments the MOT is typically loaded with 10^7 atoms of ^{88}Sr or 10^6 atoms of ^{87}Sr. At steady state, the atomic cloud has a $1/e^2$ diameter of about 2 mm and a temperature of 2 mK.

3 Frequency measurements of the $^1S_0 - {}^3P_1$ transition

The $^1S_0 - {}^3P_1$ transition at 689 nm is easy to detect since it involves the ground state. We use saturated fluorescence in an atomic beam which design was previously described in reference [28]. This atomic beam is collimated to a diameter of 4 mm and a divergence of 12 mrad (half-width at half maximum). The atomic flux is about 10^{12} at s^{-1} at an average velocity close to 500 m s^{-1}. Atoms are probed by a retro-reflected laser beam orthogonal to the atomic beam. A typical spectrum recorded for ^{88}Sr is shown in Figure 3. For frequency measurements, the laser is locked to the Lamb dip at the center of the Doppler profile.

The Zeeman sub-levels are split by a static magnetic field parallel to the atomic beam. The scan in Figure 3 is recorded with a laser polarization forming a non-zero angle with the static magnetic field of 1.5 mT. All three Zeeman components of ^{88}Sr are then visible. Frequency measurements are performed on the $m = 0 - m' = 0$ transition, insensitive to the first order Zeeman effect.

For ^{87}Sr, which possesses a nuclear spin $I = 9/2$, all possible transitions depend on the magnetic field to first order. The frequency shift of state $|^3P_1, F = 9/2, m\rangle$ is $m \times 0.8$ MHz/mT. However, one expects all Zeeman sublevels of the ground state to be equally populated in the thermal beam. In addition, since the magnetic field orientation is orthogonal to the probe laser propagation axis,

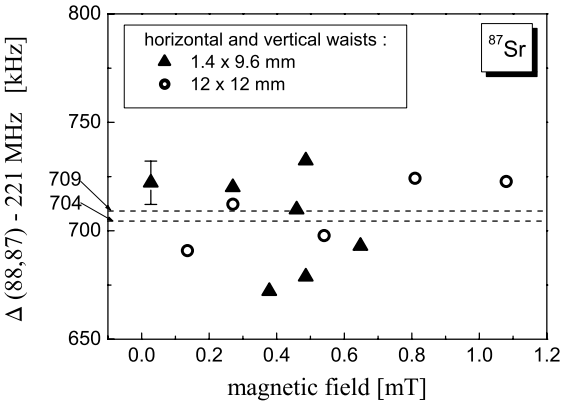

Fig. 4. Frequency measurements of the $^1S_0, F = 9/2 - {}^3P_1, F' = 9/2$ transition of ^{87}Sr referenced to the frequency of $^1S_0 - {}^3P_1$ of ^{88}Sr as a function of the magnetic field. The mean values of both sets of measurements are indicated by dashed lines. The measurements are performed with a laser power of 14 mW. The statistical uncertainty of each point is 10 kHz. The "horizontal" waist is parallel to the atomic beam.

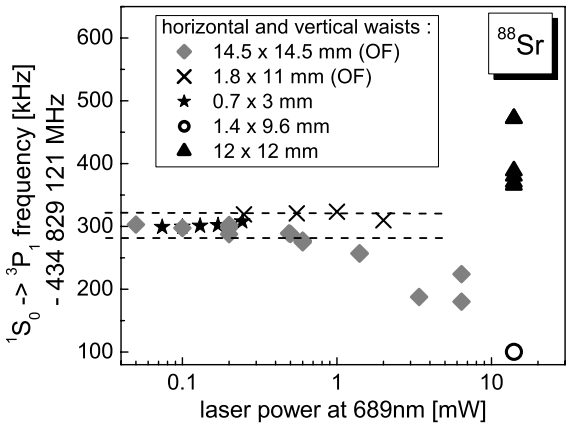

Fig. 5. Frequency measurements of $^1S_0 - {}^3P_1$ transition for ^{88}Sr, with various laser beam geometries. The horizontal waist is parallel to the atomic beam. (OF): an optical fiber is used as a spatial filter of the laser mode. The statistical error of all the measurements is less than 1 kHz.

the laser polarisation has equal σ^+ and σ^- components. One then expects the sub-Doppler structure of the resonance to be fully symmetric. Insensitivity of the frequency measurements to the magnetic field is confirmed experimentally (Fig. 4).

The main effect in the accuracy budget is the residual first order Doppler frequency shift. It is minimized by a careful alignment of the incident and retroreflected beams. First, the incident beam is collimated with a shear plate interferometer. It is aligned perpendicular to the atomic beam by equalizing to better than 20 kHz the central frequency of the Doppler profile in single pass operation and the Lamb dip frequency. Second, the laser beam is retroreflected by a cat eye allowing for a fine cancellation of the angle between the two counterpropagating laser beams. The cat eye is designed with a 15 cm focal length lens and a plane mirror located at the beam waist. It is adjusted by measuring the Lamb dip frequency as a function of the lens position: for the optimal lens-mirror distance, the frequency is independent on the transverse position of the lens. Experimentally we observe frequency shifts lower than 1 kHz for transverse displacements of the lens up to ±1 mm. First order Doppler effect also arises at high laser power from wavefront distortion due to imperfect beam collimation and aberrations [29–31]. We put an upper bound to this effect by performing frequency measurements as a function of the probe laser power with several laser beam geometries (leading to different wave fronts). The results of this study which was conducted for ^{88}Sr are summarized in Figure 5. At low laser power the measurements performed in all geometries tend towards the same frequency to within ±20 kHz, while at high power a dispersion of hundreds of kHz is observed. Our final value for ^{88}Sr is the mean value of the measurements performed at a power below 1 mW, to which we attribute a conservative error bar of 20 kHz: 434 829 121 300 (20) kHz. It is in good agreement with the measurement performed simultaneously by Ferrari et al. [32] (434 829 121 311 (10) kHz).

Table 1. $^1S_0 - {}^3P_1$ atomic frequencies. (a) Direct measurements. (b) Values computed from the measurements reported here and from the $^3P_1$ hyperfine constants given in reference [33].

	$^1S_0 - {}^3P_1$	Frequency (kHz)	
^{88}Sr	$J = 0 - J' = 1$	434 829 121 300 (20)	(a)
^{87}Sr	$F = 9/2 - F' = 7/2$	434 830 473 270 (55)	(b)
	$F = 9/2 - F' = 9/2$	434 829 343 010 (50)	(a)
	$F = 9/2 - F' = 11/2$	434 827 879 860 (55)	(b)

For ^{87}Sr frequency measurements have not been done at these low laser powers. Due to its small natural abundance (7%) and to the Zeeman degeneracy of the ground state the sub-Doppler structure is hardly detectable in the absence of saturation broadening. The atomic frequency is obtained by comparison to ^{88}Sr: at high laser power, we alternate measurements of the ^{87}Sr and ^{88}Sr resonances. We have checked that the difference between both atomic frequencies does not depend on the laser beam geometry to within 50 kHz (Fig. 4). Only the hyperfine component of ^{87}Sr with $F' = 9/2$ has been measured with this technique thanks to its small frequency difference with the ^{88}Sr transition. Since the hyperfine structure of the $^3P_1$ state of ^{87}Sr is very well-known [33] this particular measurement allows the determination of the two other hyperfine components (see Tab. 1). One can also extract the isotope shift of state $^3P_1$, $\Delta_{87,88}[^3P_1] = 62\,150\,(70)$ kHz, with an accuracy improvement by more than one order of magnitude [34,35].

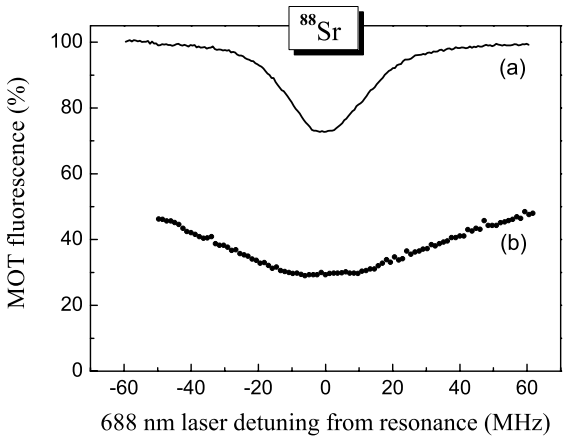

Fig. 6. Relative MOT fluorescence signals obtained when a 688 nm laser is swept around the $^3P_1 - {}^3S_1$ transition of ^{88}Sr. Measurements performed with a 0.9 mm beam waist radius and laser intensities at the center of the beam of (a) $I_{688} = 0.2$ mW cm^{-2} and (b) $I_{688} = 51$ mW cm^{-2}. The MOT has a $1/e^2$ diameter of 2 mm.

4 Frequency measurements of the $^3P_1 - {}^3S_1$ transition

Measurements of the $^3P_1 - {}^3S_1$ transition at 688 nm are performed with the cold atoms in the MOT in which the $^3P_1$ state is slightly populated. Indeed, while cycling on the $^1S_0 - {}^1P_1$ transition, atoms occasionally decay to $^1D_2$ by spontaneous emission (Fig. 1). This state has a lifetime of 0.3 ms and two main decay channels to $^3P_1$ and $^3P_2$, with respective branching ratios 67% and 33% [36]. Atoms reaching $^3P_1$ decay back to the ground state fast enough that they are kept in the trap: altogether this radiative cascade has a duration of a few hundred microseconds during which atoms travel a distance smaller than the MOT size. On the other hand atoms in the metastable $^3P_2$ state are lost for our experiment which limits the lifetime of the MOT to 30 to 50 ms, depending on the trapping laser saturation.

The $^3P_1 - {}^3S_1$ transition is detected by modifying this radiative process. If a laser resonant to one of the $^3P_1 - {}^3S_1$ transitions is added to the trap, atoms in the corresponding $^3P_1$ state are pumped to $^3P_2$ and $^3P_0$ metastable states. They escape the trap instead of decaying back to the ground state. This additional loss mechanism decreases the trapped atom number. Figure 6 shows the relative MOT fluorescence (at 461 nm) as a function of the 688 nm laser detuning from the $^3P_1 - {}^3S_1$ resonance of ^{88}Sr. Similar resonances are obtained with all hyperfine components of ^{87}Sr. It should be noted that although the relative population of the $^3P_1$ state is lower than 10^{-3}, the signal is very large indeed. The decrease of the MOT blue fluorescence can reach 40% for ^{87}Sr and 70% for ^{88}Sr at sufficiently high laser intensity.

Atoms are probed in a standing wave configuration by retroreflecting the 688 nm laser beam which shines the trapped atoms. The two counterpropagating beams are aligned to better than 1 mrad. The residual Doppler effect due to a possible asymmetry of the velocity distribution of the trapped atoms is well below 1 kHz. We have studied the contrast and width of the resonances as a function of the 688 nm laser intensity for probe beam waists ranging from 0.75 to 6 mm. Theoretical values can be simply derived from the rate equations of the MOT dynamics if one assumes that the capture process is not affected by the probe beam. We observe a strong discrepancy between experimental data and the model. The experimental resonance width is about ten times smaller than expected. Furthermore, the required laser intensity for which the contrast is half its maximal value is two orders of magnitude higher than predicted.

This shows that the effective laser intensity is much smaller than its value in the model. A significant fraction of the atoms contributing to the signal are presumably pumped at the edge of the probe beam. They escape the trap before reaching the central region of the trap. An accurate model accounting for this effect would require a good knowledge of the spatial and velocity distributions of the atoms during capture which is a hard task for a MOT loaded with a Zeeman slower.

The main consequence of numerous atoms being excited away from the trap center is a high sensitivity of the frequency measurements to the Zeeman effect induced by the MOT magnetic field. The magnetic field gradient is 1.8 mT/cm and its effect on the measured frequency is difficult to evaluate because the Zeeman structure is not resolved in the experiment. The actual resonance shape and central frequency then depends on the laser polarisation and on hardly known parameters such as the position of the MOT with respect to the zero of the magnetic field, the population of the various Zeeman sub-levels and the atom spatial distribution in the capture process. Our uncertainties are deduced from experimental observations as described in the next paragraphs. Frequencies of the atomic resonances at 688 nm could be obtained with an accuracy of 300 kHz and 500 kHz for ^{87}Sr and ^{88}Sr respectively. ^{88}Sr is more sensitive to the Zeeman effect due to its higher Landé factors (see Tab. 7).

Figure 7 shows the measured frequency of the ^{88}Sr resonance as a function of the MOT magnetic field gradient for various probe polarisations. For each measurement the probe laser is locked to the resonance with a square frequency modulation, a technique which is sensitive to an eventual asymmetry of the resonance. Although measurements with different polarizations come closer and closer while decreasing the field gradient, extrapolation to zero is not perfect. We attribute this behaviour to the asymmetry of the resonances for polarizations other than the one labelled Polar1 (Fig. 8). For this polarization, the resonance is nearly symmetric and the sensitivity to the Zeeman effect is minimal (300 kHz/[mT/cm]). For both ^{87}Sr and ^{88}Sr, we take as a final frequency the extrapolated value at zero field of the measurements performed with Polar1. The final error bar reflects the dispersion of the various zero field extrapolations. For ^{87}Sr, we observe a smaller dependence of the frequency on the MOT field gradient. Among all the ^{87}Sr transitions at 688 nm,

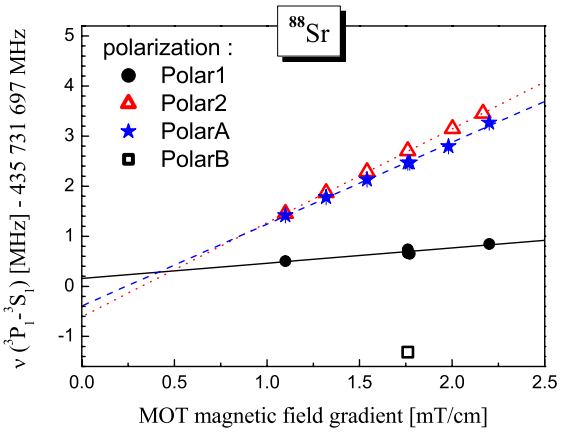

Fig. 7. Frequency shifts due to first order Zeeman effect induced by the MOT magnetic field. Measurements shown here are performed for the $^3\mathrm{P}_1 - {}^3\mathrm{S}_1$ transition of ^{88}Sr with various probe laser polarizations. Polar1 (PolarA) is perpendicular to Polar2 (PolarB). The laser intensity at the center of the beam is 0.7 mW cm^{-2}. Typical resolution of the frequency measurements is 20 kHz.

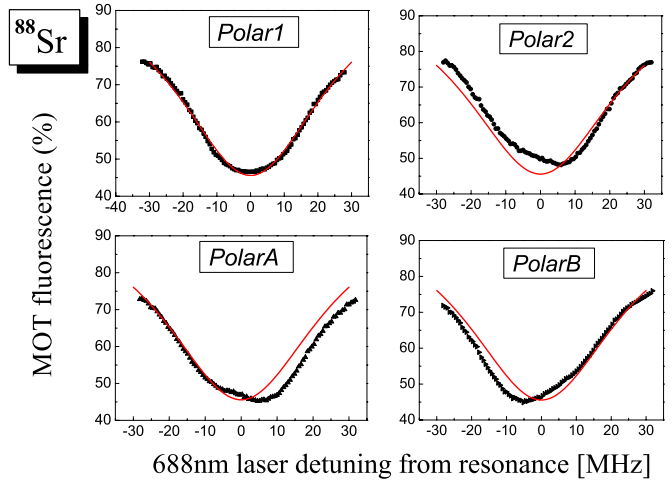

Fig. 8. $^3\mathrm{P}_1 - {}^3\mathrm{S}_1$ resonances of ^{88}Sr observed for various laser polarizations. Continuous lines in all plots represent a fit of the resonance detected with Polar1 (see text).

the highest dependency was observed for $^3\mathrm{P}_1, F = 7/2 - {}^3\mathrm{S}_1, F' = 9/2$: 150 kHz/[mT/cm] in polarization Polar1.

The effect of the magnetic field gradient can also be seen by varying the 688 nm laser intensity (Fig. 9). At increasing laser powers atoms further and further away from the trap center (where the magnetic field is higher) contribute to the signal. In order to minimize this effect, the final frequency is extrapolated from measurements done at low laser intensity only, about 1 mW cm^{-2}.

In Table 2 are reported the frequencies obtained for all transitions at 688 nm[1]. These measurements can be partly

[1] The particular 600 kHz uncertainty attributed to the $^3\mathrm{P}_1, F = 7/2 - {}^3\mathrm{S}_1, F' = 9/2$ transition is due to the fact that this resonance is less than 100 MHz away from the nearest mode of the reference Fabry-Perot cavity. In this case, the offset phase lock loop is disturbed and the spectrum of the probe laser is slightly asymmetric.

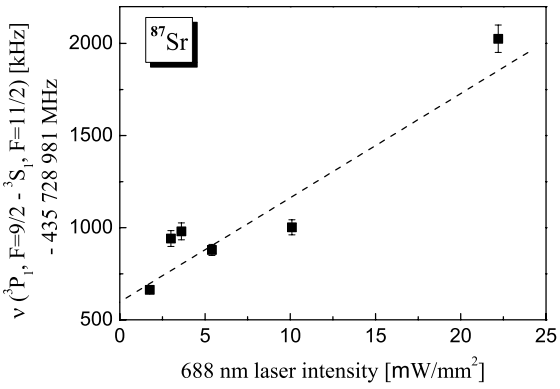

Fig. 9. Frequency shifts measured as a function of the laser intensity. Measurements performed on the $^3\mathrm{P}_1, F = 9/2 - {}^3\mathrm{S}_1, F = 11/2$ transition of ^{87}Sr with a laser waist radius of 0.9 mm and a MOT field gradient of 1.8 mT/cm.

Table 2. $^3\mathrm{P}_1 - {}^3\mathrm{S}_1$ frequency measurements.

	$^3\mathrm{P}_1 - {}^3\mathrm{S}_1$	Frequency (kHz)
^{88}Sr	$J = 1, J' = 1$	435 731 697 200 (500)
^{87}Sr	$F = 7/2 - F' = 7/2$	435 733 271 100 (600)
	$F = 7/2 - F' = 9/2$	435 730 832 300 (300)
	$F = 9/2 - F' = 7/2$	435 734 401 750 (300)
	$F = 9/2 - F' = 9/2$	435 731 962 700 (300)
	$F = 9/2 - F' = 11/2$	435 728 981 600 (300)
	$F = 11/2 - F' = 9/2$	435 733 425 800 (300)
	$F = 11/2 - F' = 11/2$	435 730 444 900 (300)

Table 3. For ^{87}Sr: frequency splitting between hyperfine levels $|^3\mathrm{P}_1, F_1\rangle$ and $|^3\mathrm{P}_1, F_2\rangle$, computed with the measurements at 688 nm involving the hyperfine level $|^3\mathrm{S}_1, F'\rangle$. Uncertainties of individual measurements are conservatively added linearly: although the Zeeman effects are expected to be quite different for different transitions (because of the Landé factors) they are certainly not independent on each other.

$F_1 - F_2$	This work via $\lvert^3S_1, F'\rangle$	This work kHz	Ref. [33] kHz
$7/2 - 9/2$	7/2	1 130 650 (800)	1 130 260 (20)
	9/2	1 130 400 (600)	
$9/2 - 11/2$	9/2	1 463 100 (600)	1 463 150 (20)
	11/2	1 463 300 (600)	
$7/2 - 11/2$	9/2	2 593 500 (600)	2 593 410 (20)

cross-checked by extracting the accurately known hyperfine splitting of the $^3\mathrm{P}_1$ state of ^{87}Sr [33]. Values are reported in Table 3. The agreement between values deduced from our measurements via different $^3\mathrm{S}_1, F'$ states on the one side and between our values and those of reference [33]

on the other side, strongly assesses the conservativeness of our uncertainties.

Frequency measurements of $^1S_0 - {}^3P_1$ and $^3P_1 - {}^3S_1$ transitions give the isotope shift, $\Delta_{87,88}\,[^3S_1]$ (referenced to the ground state), and the hyperfine constants A and B of the $^3S_1$ state:

$$\Delta_{87,88}\,[^3S_1] = 54.9\ (3)\ \text{MHz}$$
$$A\,[^3S_1] = -542.0\ (1)\ \text{MHz}$$
$$B\,[^3S_1] = -0.1\ (5)\ \text{MHz}.$$

To our knowledge, these parameters had never been measured before this work. The value of the electric quadrupole hyperfine constant B is compatible with zero as expected when both valence electrons are in s configurations ($5s6s$) [37].

5 Frequency measurements of the $^3P_0 - {}^3S_1$ transition

A direct detection of the $^3P_0 - {}^3S_1$ transition by the previous technique is not possible. Unlike $^3P_1$, $^3P_0$ is not populated in the MOT. We have performed the measurement in two steps. First, we induce a light shift on the $^3P_1 - {}^3S_1$ transition with a 679 nm laser close to the $^3P_0 - {}^3S_1$ resonance (see Fig. 1). This allows the determination of the frequency of the atomic transition at 679 nm to better than 1 MHz. In a second step, we use coherent population trapping resonances in the $\{^3P_0, {}^3P_1, {}^3S_1\}$ Λ system for a direct measurement of the $^3P_0 - {}^3P_1$ fine structure splitting. This second step which could only be applied to ^{87}Sr, leads to an uncertainty of 50 kHz on the fine structure measurement.

For both steps, the two sets of lasers as described in Section 2 are simultaneously used. At the MOT location the beam waist radii of the probe lasers (ECLD2 in Fig. 2) are $w_{679} = 1.3$ mm and $w_{688} = 0.9$ mm respectively. 679 nm and 688 nm reference lasers (ECLD1) are locked to two modes of the same high finesse cavity. From absolute frequency measurements of one of the modes, the frequency of the other one can be inferred to better than 1 kHz. It has been checked with the femtosecond frequency chain by alternating frequency measurements of the 679 nm and 688 nm lasers or by directly measuring their frequency difference.

Light shift measurements are plotted in Figure 10. The 679 nm laser induces a frequency dependent light shift of $^3S_1$ which is deduced from measurements of the $^3P_1 - {}^3S_1$ transition with the 688 nm laser. The $^3P_0 - {}^3S_1$ atomic frequency corresponds to the center of symmetry of the light shift curve. For the signal to be as large as possible the total available power at 679 nm is used. A 2.4 mW laser beam shines the trapped atoms in a standing wave configuration. In order to minimize the number of atoms being excited far from the MOT center the 688 nm laser has a low intensity, typically $I_{688} = 0.2$ mW cm^{-2}. It should be noted that the measured light shift is about 10 times smaller than the value derived from a simple

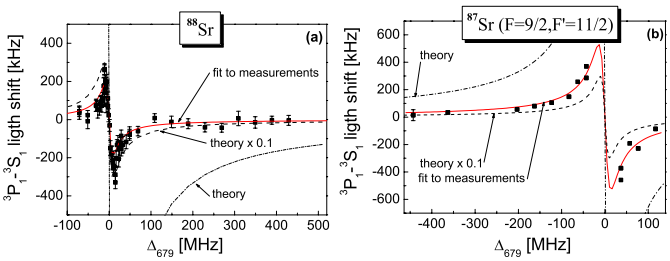

Fig. 10. Light shift of the $^3P_1 - {}^3S_1$ transition induced by the 679 nm laser as a function of Δ_{679}, the frequency detuning from $^3P_0 - {}^3S_1$ resonance. The zero on the vertical axis corresponds to the $^3P_1 - {}^3S_1$ frequency measured in the absence of the 679 nm laser. Measurements are performed with mean intensities $I_{679} = 180$ mW cm^{-2} and $I_{688} = 0.2$ mW cm^{-2}. Dashed lines represent the theoretical light shift for an atom modelled as a two-level system with a natural linewidth $\Gamma^*/2\pi = 15.9$ MHz and a Rabi frequency $\Omega_{679}/2\pi = 16.3$ MHz.

two-level atom model assuming a transition natural width $\Gamma^* = \Gamma_{679} + \Gamma_{688} + \Gamma_{707} = 2\pi \times 15.9$ MHz and a Rabi frequency $\Omega/2\pi = 16.3$ MHz.

For ^{88}Sr (Fig. 10a) the frequency of the resonance at 679 nm is obtained with a statistical uncertainty of 400 kHz. We add a 500 kHz uncertainty due to the Zeeman effect and end up with:

$$^{88}\text{Sr:}\quad {}^3P_0 \rightarrow {}^3S_1 \quad \nu = 441\,332\,751.3\,(0.7)\ \text{MHz}.$$

A more accurate measurement can be performed with coherent population trapping [38]. Consider the $\{^3P_0, {}^3P_1, {}^3S_1\}$ Λ system coupled with the lasers at 679 nm and 688 nm. When the frequency difference between both lasers matches the $^3P_0 - {}^3P_1$ fine structure splitting, there exists a linear superposition $|\psi_{NC}\rangle$ of the two $^3P_{0,1}$ states which is not coupled to $^3S_1$. Let $|\psi_C\rangle$ be the superposition of $^3P_0$ and $^3P_1$ which is orthogonal to $|\psi_{NC}\rangle$. Atoms decaying from $^1D_2$ are projected either onto $|\psi_{NC}\rangle$ or onto $|\psi_C\rangle$. Atoms in $|\psi_C\rangle$ are essentially pumped to $^3P_2$ and escape the trap (see Fig. 1) while atoms projected onto the dark state $|\psi_{NC}\rangle$ end up in the atomic ground state because of the instability of $^3P_1$. These atoms recover the trapping process.

In Figure 11 is plotted the MOT fluorescence as the 688 nm laser is swept around the $^3P_1, F = 9/2 - {}^3S_1, F' = 11/2$ transition of ^{87}Sr. For the signal shown in Figure 11a the 688 nm laser alone is sent to the atoms. As depicted in the previous section, a decrease in the MOT fluorescence is observed as the 688 nm laser pumps atoms from $^3P_1$ to $^3P_0$ and $^3P_2$. In Figures 11b and 11c, the 679 nm laser also shines the trap and the CPT resonance is observed. When the 679 nm laser is tuned exactly onto the $^3P_0, F = 9/2 - {}^3S_1, F' = 11/2$ transition, the CPT resonance is detected as an increase of the MOT fluorescence at the center of the broad 688 nm resonance (Fig. 11b). This increase is due to the atoms projected onto the dark state $|\psi_{NC}\rangle$ which decay to the ground state and recover the trapping process. If we gradually increase the 679 nm laser detuning, the CPT resonance moves sidewards and reverses sign when it reaches the wings of the 688 nm

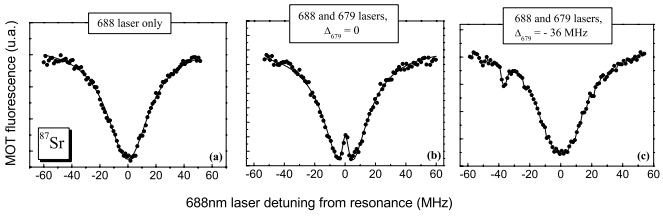

Fig. 11. MOT fluorescence signals as a function of the 688 nm laser detuning from the $^3\mathrm{P}_1, F = 9/2 - {}^3\mathrm{S}_1, F' = 11/2$ transition of ^{87}Sr. (a) 688 nm laser only; (b) and (c) with an additional 679 nm laser at fixed frequency, detuned by Δ_{679} from $^3\mathrm{P}_0, F = 9/2 - {}^3\mathrm{S}_1, F' = 11/2$ resonance. The linewidth of the CPT resonance is 3 MHz due to power and Zeeman broadening. Measurements recorded with laser intensities $I_{688} = 1.3\ \mathrm{mW\,cm^{-2}}$ and $I_{679} = 130\ \mathrm{mW\,cm^{-2}}$.

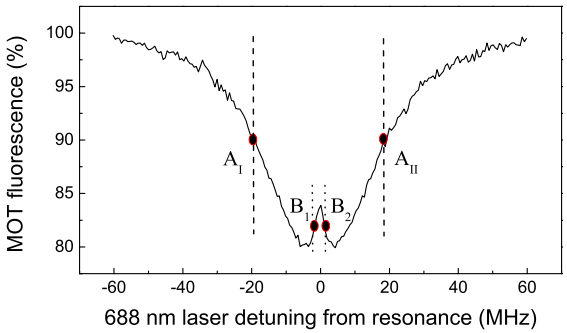

Fig. 12. 688 nm and 679 nm lasers are both locked by frequency modulation of the 688 nm laser. From fluorescence measurements at frequencies A_I et A_{II} the 688 nm laser is locked to $^3\mathrm{P}_1 - {}^3\mathrm{S}_1$ resonance. Measurements at B_1 et B_2 are used to locked the 679 nm to $^3\mathrm{P}_0 - {}^3\mathrm{S}_1$. Experiment performed tuning the 688 nm laser around the $^3\mathrm{P}_1, F = 9/2 - {}^3\mathrm{S}_1, F' = 11/2$ resonance of ^{87}Sr.

resonance (Fig. 11c). We then detect atoms projected onto $|\psi_C\rangle$ which are optically pumped to $^3\mathrm{P}_2$, a process which increases the MOT losses as compared to the situation with the 688 nm laser alone.

The CPT resonance allows for a direct measurement of the $^3\mathrm{P}_0, F = 9/2 - {}^3\mathrm{P}_1, F' = 9/2$ fine structure splitting of ^{87}Sr. Three measurements have been performed with each of the $^3\mathrm{S}_1$ hyperfine levels as a third state in the Λ system. For ^{88}Sr and other $^3\mathrm{P}_1$ hyperfine states of ^{87}Sr, the CPT resonances are blurred due to the higher sensitivity of the involved states to magnetic field. Only a deformation of the 688 nm resonance has been observed which did not allow for accurate measurements.

The fine structure measurements are performed with the frequency of both 688 nm and 679 nm lasers locked to the atomic signal. Three digital servo loops run in parallel. Servo A locks the 688 nm laser frequency to the $^3\mathrm{P}_1 - {}^3\mathrm{S}_1$ transition. This is done by alternating measurements at frequencies A_I and A_{II} indicated in Figure 12. With servo B, the 688 nm laser is locked onto the CPT peak thanks to measurements at frequencies B_1 and B_2 (Fig. 12). Finally servo C controls the frequency of the 679 nm laser so as to equalize the frequencies of servos

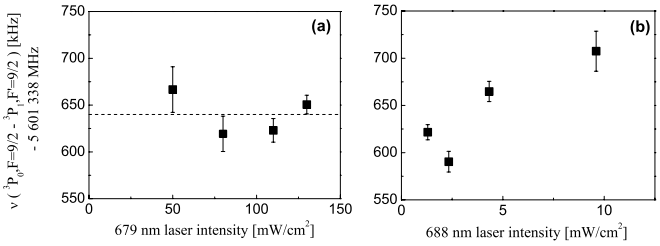

Fig. 13. Frequency measurements of $^3\mathrm{P}_0, F = 9/2 - {}^3\mathrm{P}_1, F = 9/2$ splitting as a function of (a) the 679 nm laser intensity and (b) the 688 nm laser intensity. Both lasers are locked to resonance: the 679 nm laser to $^3\mathrm{P}_0, F = 9/2 - {}^3\mathrm{S}_1, F' = 11/2$ and the 688 nm laser to $^3\mathrm{P}_1, F = 9/2 - {}^3\mathrm{S}_1, F' = 11/2$.

A and B. Measurements for servo A and B are interlaced with variable durations. The fine structure measurement is deduced from the difference of the average frequencies of servos A and C. A frequency resolution of 10 kHz is achieved in a few minutes of averaging.

With this scheme, both lasers are locked on their respective atomic resonance which enables light shift free measurements. Indeed, no shift is observed as a function of the 679 nm laser intensity (see Fig. 13a). When the 688 nm laser intensity is increased however, we do observe a shift (Fig. 13b). As previously reported for the $^3\mathrm{P}_1 - {}^3\mathrm{S}_1$ measurements (Fig. 9), this effect is attributed to the Zeeman effect induced by the MOT field gradient. Increasing the laser intensity enhances the number of atoms excited away from the zero magnetic field region. It is to be noted that using a 679 nm laser at high intensity ($\sim$100 $\mathrm{mW\,cm^{-2}}$) does not enhance the Zeeman effect because the 688 nm laser performs the spatial selection.

Again the Zeeman effect is the dominant systematic frequency shift in this experiment. It has been shown in the previous section that it is minimized using lasers in the particular polarization Polar1 and addressing only atoms close to the center of the MOT. The sensitivity of the CPT resonance to the Zeeman effect is 5 to 6 times smaller than for the 688 nm measurements of ^{87}Sr. We attribute a 50 kHz uncertainty to the $^3\mathrm{P}_0, F = 9/2 - {}^3\mathrm{P}_1, F' = 9/2$ fine structure measurements. They have been performed via the three hyperfine levels of $^3\mathrm{S}_1$. We finally obtain:

$$\nu\,(^3\mathrm{P}_0, F = 9/2 - {}^3\mathrm{P}_1, F' = 9/2) = 5\,601\,338\,670\,(50)\ \mathrm{kHz}.$$

From this measurement and the values of Table 2 the frequency of all the $^3\mathrm{P}_0, F = 9/2 - {}^3\mathrm{S}_1, F'$ transitions are deduced (Tab. 4). The isotope shift of the $^3\mathrm{P}_0$ state can also be extracted:

$$\Delta_{87,88}\,[^3\mathrm{P}_0] = 62.9\ (1.3)\ \mathrm{MHz}.$$

We have determined all the frequencies of the $^1\mathrm{S}_0 - {}^3\mathrm{P}_1$, $^3\mathrm{P}_1 - {}^3\mathrm{S}_1$ and $^3\mathrm{P}_0 - {}^3\mathrm{S}_1$ transitions for ^{87}Sr and ^{88}Sr. From these measurements the $^3\mathrm{S}_1$ hyperfine constants and the $^3\mathrm{P}_0$, $^3\mathrm{P}_1$ and $^3\mathrm{S}_1$ isotope shifts could be extracted (Tab. 5). Frequency measurements performed for ^{88}Sr can be compared to the values of reference [39]. Authors of this reference estimate their accuracy to 0.002 nm ($\simeq$1.2 GHz)

Table 4. $^3P_0 - {}^3S_1$ atomic frequencies. (a) Direct measurement. (b) Computed from CPT measurements and values from Table 2.

	$^3P_0 - {}^3S_1$	frequency (kHz)	
^{88}Sr	$J = 0 - J' = 1$	441 332 751 300 (700)	(a)
^{87}Sr	$F = 9/2 - F' = 7/2$	441 335 740 420 (350)	(b)
	$F = 9/2 - F' = 9/2$	441 333 301 370 (350)	(b)
	$F = 9/2 - F' = 11/2$	441 330 320 270 (350)	(b)

Table 5. Isotope shifts between ^{87}Sr and ^{88}Sr (referenced to the ground state).

	$\Delta_{87,88}$ (kHz)	
$^3P_0$	62 900	(1 300)
$^3P_1$	62 150	(70)
$^3S_1$	54 900	(300)

Table 6. Comparison between our frequency measurements and values computed from Rubbmark et al. [39].

^{88}Sr	Rubbmark et al. ν(MHz)	This work ν(MHz)
$^1S_0 - {}^3P_1$	434 829 300	434 829 121.30 (0.02)
$^3P_1 - {}^3S_1$	435 731 500	435 731 697.2 (0.5)
$^3P_0 - {}^3S_1$	441 332 600	441 332 751.3 (0.7)

but notice that their values are in agreement to better than 0.0005 nm (300 MHz) with those reported in reference [40]. As shown in Table 6, it appears they are wrong by 100 MHz to 200 MHz only.

One of the goals of the above experiments was to yield an accurate knowledge of the frequency of $^1S_0 - {}^3P_0, F = 9/2$ clock transition of ^{87}Sr. We find $\nu = 429\,228\,004\,340(70)$ kHz. This indirect estimate was a decisive step toward the direct observation of this transition which we describe in the following section with more details than in [24].

6 Direct measurement of the $^1S_0 - {}^3P_0$ transition

For ^{87}Sr, the $^1S_0 - {}^3P_0$ transition at 698 nm is slightly allowed by hyperfine coupling of $^3P_0$ to $^1P_1$ and $^3P_1$. Its theoretical linewidth is estimated to 1 mHz [25,41]. Detection of such a narrow line is a technical challenge with atoms at 2 mK even if its frequency is already known. To obtain a detectable signal we have developed an original technique based on the MOT dynamics and the use of a 698 nm laser frequency sweep. The principle consists in inducing in the MOT a leak to $^3P_0$ with a 698 nm laser. Detection of a small number of atoms in this state is made difficult by the absence of cycling transition from this state. The detection of the $^1S_0 - {}^3P_0$ transition is then performed by measuring the loss induced in the MOT with the 461 nm fluorescence of the trapped atoms.

In order to excite the largest possible fraction of atoms, the 698 nm laser is used at the highest available power, 14 mW. The laser beam is sent four times through the MOT forming two standing waves. Both waves are tilted by 5 mrad with respect to each-other and by 45° with respect to vertical. Their waist radius is 1.3 mm. With these parameters, the resonance is broadened by saturation to 1.8 kHz. On the other hand, the Doppler broadening for our 2 mK atomic sample is 1.5 MHz (full width at half-maximum (FWHM)). Only one atom out of 10^3 is then expected to be resonant with the laser at a given time.

However, the MOT dynamics can lead to an amplification of the transfer rate to $^3P_0$. Indeed, with the laser parameters given above, the duration of a π pulse on the narrow transition is 0.5 ms. This is about 100 times shorter than the MOT lifetime. It is then in principle possible to enhance the fraction of excited atoms by the same factor if one accumulates atoms in $^3P_0$. The induced MOT loss should then reach several %. This works only if two conditions are fulfilled. First, the transfer rate to $^3P_0$ has to remain constant. This is at first sight not the case since the 698 nm laser excitation creates a dip in the velocity distribution of atoms in the ground state. Second, atoms once in the $^3P_0$ state have to actually escape the trapping process. If they stay resonant with the 698 nm laser frequency, they flip back to the ground state by stimulated emission. To ensure both conditions, several methods can be thought of. For instance, the MOT beams could be used to rethermalize atoms and fill the dip in the the ground state velocity distribution. For the escape condition, optical pumping to $^3P_2$ state could be performed with a laser tuned to the $^3P_0 - {}^3S_1$ resonance as in reference [42]. Alternatively, both conditions can be simultaneously fulfilled by sweeping the laser frequency. This is doable if the frequency ramp is perfectly controlled so as to not degrade the accuracy of the frequency measurements.

We have used a simpler method based on the Doppler effect induced by the acceleration of atoms by gravity. The experiment is operated sequentially. By means of acousto-optic modulators we alternate capture and cooling phases with the 461 nm lasers and probe phases with the 698 nm laser. During probe phases atoms are freely falling. Due to the 45° angle formed by the 698 nm beam and the vertical, the frequency sweep caused by gravity amounts to 10 kHz/ms. Both atoms transferred to the $^3P_0$ state and the corresponding dip in the velocity distribution of the ground state are then detuned from the laser excitation. The pulsed operation of the experiment also prevents any light shift of the ground state by the MOT beams during probe phases.

We have developed a simple model of the loss induced in the trap by excitation to $^3P_0$. We compute the transition probability for an atom probed by two counterpropagating beams of 28 mW each, hence averaging down the effect of the interference due to the 5 mrad tilt between the actual beams. We also neglect spontaneous emission and treat the atom as a two level system. For an

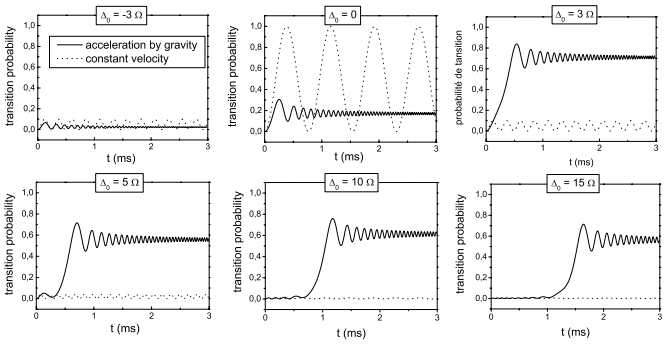

Fig. 14. Transition probabilities as a function of the interaction time for various detunings Δ_0 at $t = 0$ (with $\Omega/2\pi = 920$ Hz). Continuous lines: atoms accelerated by gravity. Dashed lines: atoms having a constant velocity.

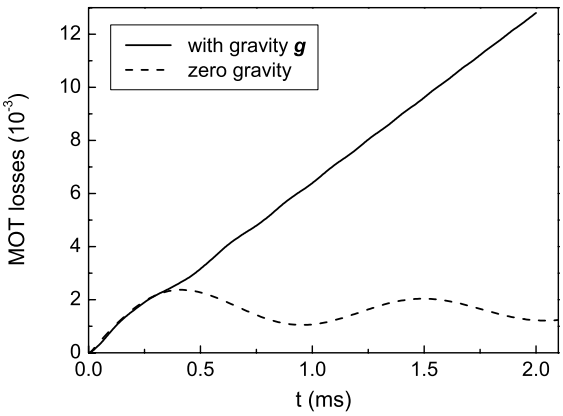

Fig. 15. Relative loss induced in the MOT as a function of the interaction time in the absence (dashed line) and in presence (solid line) of gravity.

atom of initial velocity $\vec{v}_0$ we numerically solve the optical Bloch equations with a time dependent detuning from resonance $\Delta(t)$. Accounting for the gravity acceleration $\vec{g}$ it writes down as:

$$\Delta(t) = \Delta_0 + \varepsilon\, \alpha\, t \tag{1}$$

$$\text{with :} \quad \Delta_0 = \delta + \varepsilon\, \vec{k} \cdot\, \vec{v}_0 \tag{2}$$

$$\alpha = \frac{1}{\sqrt{2}}\, \vec{k} \cdot \vec{g} \simeq 2\pi \times 10 \text{ kHz/ms}. \tag{3}$$

Here δ is the laser detuning in the laboratory frame, $\vec{k}$ the probe laser wave vector and $\varepsilon = \pm 1$ depending on the direction of the laser beam interacting with the atoms. We have neglected interferences between counterpropagating laser beams considering they address different atomic velocity classes. This is true for large enough detuning, typically $|\delta| > 10\Omega$, with Ω the Rabi frequency. Accounting for both beams would lead to a sub-Doppler structure at the center of the resonance which was not resolved experimentally.

The transition probabilities obtained for various values of Δ_0 in the case $\varepsilon = -1$ are plotted in solid lines in Figure 14. When atoms with a blue initial detuning ($\Delta_0 > 0$) are brought onto resonance by the acceleration of gravity, the transition probability rapidly increases and then tends to stabilize around a high value, for instance 0.56 when $\Delta_0 = 5\Omega$. Also shown in Figure 14 (dashed lines) is the transition probability which would be obtained in the absence of gravity, i.e. for a constant value $\Delta(t) = \Delta_0$. It is clear that if the interaction time is sufficient, a significant transition probability is obtained for a much broader range of initial atomic velocity when gravity is accounted for.

The evolution of the transition probability of an initially blue detuned atom is remindful of adiabatic rapid passage. Indeed our experimental parameters are at the edge of the adiabatic transfer condition [43]:

$$\dot{\Delta} \ll 2\, \Omega^2. \tag{4}$$

Our parameters yield:

$$\frac{\dot{\Delta}}{2\, \Omega^2} \simeq 0.94.$$

The loss induced in the MOT per probe pulse is given by the above transition probability after integration over the whole atomic velocity distribution. In Figure 15 are plotted the results obtained in the presence (solid line) and in the absence (dashed line) of gravity. At zero gravity the loss rapidly stabilizes around a small value: 1.6×10^{-3} of the total number of trapped atoms. This value is close to the intuitive value given by the ratio of saturation over Doppler broadenings. By contrast, gravity enables to induce loss in the MOT that keep increasing with the interaction time: more and more atoms are brought onto resonance due to gravity. An even faster frequency sweep would lead to a higher increase of the loss in the MOT. For instance, with a 100 kHz/ms ramp, a further increase of 40% is expected. This would however be at the cost of an experimental complication. The frequency ramp should be perfectly controlled and synchronized with the experimental time sequence.

Our time sequence consists in alternating phases of cooling and capture of 3 ms duration with probe phases of 1 ms duration. This sequence, which was experimentally optimized, results from a trade-off between the MOT capture efficiency, the ballistic expansion of the atomic cloud during probe phases, and the efficiency of excitation to $^3P_0$. From the results of our model and given the 40 ms lifetime of the MOT with this time sequence parameters, we expect a contrast of the resonance of 6%.

In Figure 16 is shown the observed $^1S_0 - ^3P_0$ resonance. The contrast is 1%, 6 times lower than the expected value. The discrepancy between experimental and expected value may have several causes. Neglecting the angle between both standing waves may lead to an overestimate of the MOT loss by a factor of nearly 2. In addition, the ballistic expansion of the atomic cloud has been neglected in the model. During probe phases, atoms are moving away from the 698 nm beam center due to their residual velocity. The actual Rabi frequency thus decreases with time. This also leads to a decrease of the transfer rate to $^3P_0$.

We have locked the 698 nm laser to the $^1S_0 - {}^3P_0$ resonance with a digital servo loop. The error signal is derived from MOT fluorescence measurements performed

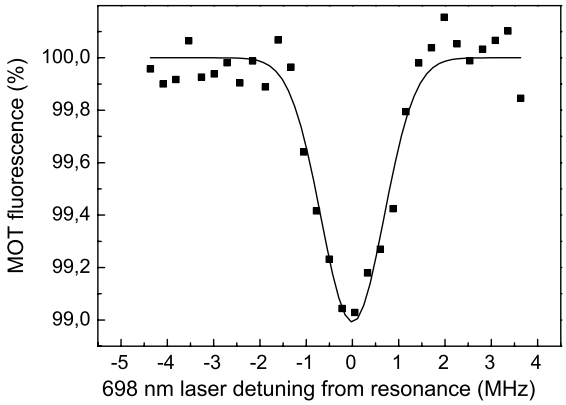

Fig. 16. Direct observation of $^1S_0 - {}^3P_0$ transition of ^{87}Sr. The line is broadened by the Doppler effect to 1.4 MHz (FWHM) due to the temperature of the atoms. The maximal value of the MOT fluorescence corresponds to 3×10^6 trapped atoms.

sequentially on both sides of the resonance. The duration of each fluorescence measurement is a multiple of the time sequence period used to probe the atoms. The error signal is integrated and fed back to the synthesizer driving the offset-phase lock of the probe laser ECLD2 (Fig. 2). The mean frequency of the measurements is 429 228 004 235 kHz with a residual statistical uncertainty of 15 kHz.

At this level, systematic effects are negligible. The residual Doppler effect is well below 1 kHz due to the standing wave configuration. The Zeeman effect amounts to less than 1 kHz in spite of the MOT field gradient since Landé factors of $^1S_0$ and $^3P_0$ states are extremely small (Tab. 7). Finally measurements performed with imperfect extinction by the acousto-optic modulators show that the residual light shift by the 461 nm light is also below 1 kHz. The Doppler profile being shifted from the atomic resonance by the recoil frequency [44], the measured mean frequency has to be corrected by 4.7 kHz[2]. We finally obtain:

$$\nu\,(^1S_0 - {}^3P_0) = 429\,228\,004\,230\,(15)\ \text{kHz}.$$

This value is in agreement with the indirect determination, the difference between both frequencies being 1.4 σ.

Conclusion

We have measured the frequency of the $^1S_0 - {}^3P_1$ (Tab. 1), $^3P_1 - {}^3S_1$ (Tab. 2) and $^3P_0 - {}^3S_1$ (Tab. 4) optical transitions for both strontium isotopes ^{87}Sr and ^{88}Sr. The reported accuracy is in the 100 kHz range, an improvement by three orders of magnitude as compared to previous values [39]. This was made possible by the versatility of femto-second laser based optical frequency measurements and in turn nicely illustrates the potential of this technique. It is worth noting that with traditional harmonic frequency chain measurements, four quite different (and complex) experiments should have been built, one for each specific wavelength: 679 nm, 688 nm, 689 nm and finally 698 nm.

These measurements lead to a better knowledge of atomic Sr yielding accurate values of the hyperfine structure parameters of state $^3S_1$ and of the isotope shift of states $^3P_0$, $^3P_1$ and $^3S_1$. Thanks to the indirect determination of the energy of state $^3P_0$ the $^1S_0 - {}^3P_0$ clock transition of ^{87}Sr could be directly detected. Although this transition is extremely forbidden (its natural linewidth is 1 mHz) we have been able to observe it on a sample at a temperature of 2 mK by making use of the magneto-optical trap dynamics. We have induced a leak in the MOT to state $^3P_0$ which enhanced the contrast of the transition by one order of magnitude as compared to simple saturation broadening. We performed a direct measurement of the clock transition frequency which is found in agreement with the indirect determination. The technique used here could be applied to detect other strongly forbidden lines like the slightly broader $^1S_0 - {}^3P_0$ transition of fermionic Yb. The lifetime of Yb atoms in a MOT using the $^1S_0 - {}^3P_1$ transition [45] is typically two orders of magnitude longer than our Sr MOT and the contrast of the resonance could then approach 100%.

Although this clock transition is interesting in itself, whatever the scheme used to probe the atoms, the frequency measurement of the $^1S_0 - {}^3P_0$ of ^{87}Sr is the first step towards the construction of a new generation of atomic clocks: optical clocks with trapped atoms [25, 42]. It seems realistic with these clocks to reach in a close future a fractional frequency instability around $10^{-16}\tau^{-1/2}$ [27] together with an accuracy in the 10^{-17} range [25].

We thank Ouali Acef, Sébastien Bize, André Clairon, Michel Lours, Giorgio Santarelli and J.-J. Zondy for helpful discussions, and the optoelectronic group of the university of Bath (UK) for providing the photonic crystal fiber of the frequency chain. A.B. acknowledges his grant from the european Research Training Network CAUAC. BNM-SYRTE is Unité Associée au CNRS (UMR 8630).

Annexe: Landé factors

Table 7. Landé factors.

	$^1S_0$		$^3P_0$		$^1P_1$			
	^{87}Sr	^{88}Sr	^{87}Sr	^{88}Sr	^{87}Sr			^{88}Sr
F	9/2	0	9/2	0	7/2	9/2	11/2	1
g_F	-1.3×10^{-4}	0	-6×10^{-5}	0	−2/9	4/99	2/11	1

	$^3P_1$				$^3S_1$			
	^{87}Sr			^{88}Sr	^{87}Sr			^{88}Sr
F	7/2	9/2	11/2	1	7/2	9/2	11/2	1
g_F	−1/3	2/33	3/11	3/2	−4/9	8/99	4/11	2

[2] The value published in [24] was erroneously not corrected for the recoil.

References

1. See, articles in *The Hydrogen Atom*, edited by G.F. Bassani, M. Inguscio, T.W. Hänsch (Springer-Verlag, Berlin, 1989)
2. T. Udem et al., Phys. Rev. Lett. **79**, 2646 (1997)
3. C. Schwob et al., Phys. Rev. Lett. **82**, 4960 (1999)
4. D.J. Berkeland, E.A. Hinds, M.G. Boshier, Phys. Rev. Lett. **75**, 2470 (1995)
5. P. Cancio Pastor et al., Phys. Rev. Lett. **92**, 023001 (2004)
6. in *Proceedings of the Sixth Symposium on frequency standards and metrology*, edited by P. Gill (World Scientific, Singapore, 2002)
7. J.-P. Uzan, Rev. Mod. Phys. **75**, 403 (2003)
8. S. Bize et al., Phys. Rev. Lett. **82**, 150802 (2003)
9. H. Marion et al., Phys. Rev. Lett. **82**, 150801 (2003)
10. M. Fischer et al., Phys. Rev. Lett. **92**, 230802 (2004)
11. E. Peik et al., Phys. Rev. Lett. **91**, 170801 (2004)
12. T. Udem, J. Reichert, R. Holzwarth, T.W. Hänsch, Phys. Rev. Lett. **82**, 3568 (1999)
13. A. Wicht, J.M. Hensley, E. Sarajlic, S. Chu, in *Sixth Symposium on frequency standards and metrology*, edited by P. Gill (World Scientific, Singapore, 2002)
14. S. Gupta, K. Dieckmann, Z. Hadzibabic, D.E. Pritchard, Phys. Rev. Lett. **89**, 140401 (2002)
15. R. Battesti et al., Phys. Rev. Lett. **92**, 253001 (2004)
16. D.A. Jennings et al., Opt. Lett. **8**, 136 (1983)
17. A. Clairon, B. Dahmani, A. Filimon, J. Rutman, IEEE Trans. Instr. Meas. **34**, 265 (1985)
18. T. Andreae et al., Phys. Rev. Lett. **69**, 1923 (1992)
19. F. Nez et al., Phys. Rev. Lett. **69**, 2326 (1992)
20. H. Schnatz et al., Phys. Rev. Lett. **76**, 18 (1996)
21. J.E. Bernard et al., Phys. Rev. Lett. **82**, 3228 (1999)
22. A. Bauch, H.R. Telle, Rep. Prog. Phys. **65**, 789 (2002)
23. S.T. Cundiff, J. Ye, Rev. Mod. Phys. **75**, 325 (2003)
24. I. Courtillot et al., Phys. Rev. A **68**, R030501 (2003)
25. H. Katori, M. Takamoto, V.G. Pal'chikov, V.D. Ovsiannikov, Phys. Rev. Lett. **91**, 173005 (2003)
26. R.W.P. Drever et al., App. Phys. B **31**, 97 (1983)
27. A. Quessada et al., J. Opt. B: Quant. Semiclass. Opt. **5**, S150 (2003)
28. I. Courtillot et al., Opt. Lett. **28**, 468 (2003)
29. J.L. Hall, C.J. Bordé, Appl. Phys. Lett. **29**, 788 (1976)
30. J. Ishikawa, F. Riehle, J. Helmcke, Ch.J. Bordé, Phys. Rev. A **49**, 4794 (1994)
31. P. Lemonde et al., in *Proc. of Frequency Control Symposium* (IEEE, Pasadena, 1998)
32. G. Ferrari et al., Phys. Rev. Lett. **91**, 243002 (2003)
33. G. zu Putlitz, Z. Phys. **175**, 543 (1963)
34. F. Buchinger, R. Corriveau, E.B. Ramsay, Phys. Rev. C **32**, 2058 (1985)
35. A.A. Celikov, A.M. Akulshin, V.L. Velichanski, A.S. Zibrov, Laser Phys. **5**, 739 (1995)
36. C.W. Bauschlicher, S.R. Langhoff, H. Patridge, J. Phys. B **18**, 1523 (1985)
37. I. Sobelman, *Atomic spectra and radiative transitions* (Springer-Verlag, 1979)
38. G. Alzetta, A. Gozzini, L. Moi, G. Orriols, Nuovo Cim. B **36**, 5 (1976)
39. J.R. Rubbmark, S.A. Borgström, Phys. Scr. **18**, 196 (1978)
40. F.J. Sullivan, Ph.D. thesis, Univ. of Pittsburgh, Pennsylvania, USA (1938)
41. S.G. Porsev, A. Derevianko, Phys. Rev. A **69**, 042506 (2004).
42. M. Takamoto, H. Katori, Phys. Rev. Lett. **91**, 223001 (2003)
43. A. Messiah, *Quantum Mechanics* (North-Holland, Amsterdam, 1962), Vol. 2
44. W. Demtröder, *Laser Spectroscopy* (Springer, New York, 1981)
45. T. Kuwamoto, K. Honda, Y. Takahashi, T. Yabuzaki, Phys. Rev. A **60**, R745 (1999)